Vertical variations in O_3 concentrations before and after a gust front passage

Lisa S. Darby, Robert M. Banta, W. Alan Brewer, and William D. Neff
National Oceanic and Atmospheric Administration/Environmental Technology Laboratory, Boulder, Colorado, USA

Richard D. Marchbanks, Brandi J. McCarty, Christoph J. Senff, and Allen B. White
Cooperative Institute for Research in the Environmental Sciences, University of Colorado, Boulder, Colorado, USA

Wayne M. Angevine and Eric J. Williams
National Oceanic and Atmospheric Administration/Aeronomy Laboratory, Boulder, Colorado, USA

Received 26 June 2001; revised 12 November 2001; accepted 18 November 2001; published 11 July 2002.

[1] Two consecutive increases in surface ozone, occurring after the cessation of photochemical ozone production, are investigated. A unique suite of instruments, including an ozone profiling lidar, a Doppler lidar, surface chemistry sensors, surface meteorological sensors, and a radar wind profiler, was deployed during the Southern Oxidants Study of 1999 in Nashville, Tennesee. Time series of ozone at 10, 405, and 1035 m above ground level (AGL) on 22 June 1999 showed variations in the vertical gradient of ozone over the course of the afternoon and evening. Analysis of time series of vertical velocity at 8 m AGL and its standard deviation, the variance in Doppler lidar calculated horizontal wind speed from near the surface to 500 m AGL, wind profiles, and meteorological surface station data, revealed mechanisms responsible for these changes in ozone. An early evening rise in surface ozone occurred with the passage of a thunderstorm gust front. Analysis showed that downward mixing of ozone-rich air from a residual layer (RL) of ozone above 400 m caused a sharp rise in ozone at the surface and a decrease of ozone in the RL. Doppler lidar measurements showed details of the postgust front wind flow, such as the depth of the air mass behind the front, the turbulent wake region, and inferred vertical velocities throughout a layer several hundred meters deep. The second rise in surface ozone was caused by turbulent mixing due to elevated directional wind shear, which mixed ozone-rich air down to the surface. *INDEX TERMS:* 3307 Meteorology and Atmospheric Dynamics: Boundary layer processes; 3360 Meteorology and Atmospheric Dynamics: Remote sensing; 3329 Meteorology and Atmospheric Dynamics: Mesoscale meteorology; *KEYWORDS:* Doppler lidar, ozone lidar, gust front, nocturnal ozone increase, Southern Oxidants Study, vertical ozone distribution

1. Introduction

[2] As photochemical production of ozone subsides in late afternoon and ceases in the evening, ozone concentrations measured near the surface typically decrease as a result of deposition and NO_x titration by NO. Occasionally, events occur that interrupt this decline and produce a temporary increase in ozone. Such increases in surface ozone values after photochemical production of ozone has ceased have been previously studied [e.g., *Corsmeier et al.*, 1997; *Reitebuch et al.*, 2000; *Zurita and Castro*, 1983]. The increases in ozone concentrations were either presumed or shown from ozonesonde data to be caused by downward mixing of ozone-rich air. The downward mixing resulted from turbulence produced by either a low-level jet (LLJ) [*Corsmeier et al.*, 1997; *Reitebuch et al.*, 2000], a cold front passage [*Reitebuch et al.*, 2000] or the breakdown of stability of the planetary boundary layer (PBL) due to bursts of turbulence [*Nappo*, 1991]. Whereas hourly ozonesonde data were available in the work of *Corsmeier et al.* [1997], continuous time series of ozone concentrations above the ground were not available for any of these studies listed above.

[3] The Southern Oxidants Study (SOS), a multiagency collaboration, conducted an experiment based in Nashville, Tennessee, in June and July 1999. The scientific objectives were numerous, but the fundamental goal was to understand the formation and accumulation of pollution in the southeastern region of the United States. With the objective of defining effective control strategies for ozone and particulate matter, data from SOS 1999 are expected to improve our understanding of both the physics and chemistry of the atmosphere. Regional issues, such as power plant plume transport, were investigated by instrumented aircraft and a radar wind profiler network. Documenting chemical processes throughout the diurnal cycle, across regional and

0148-0227/02/2001JD000996$09.00

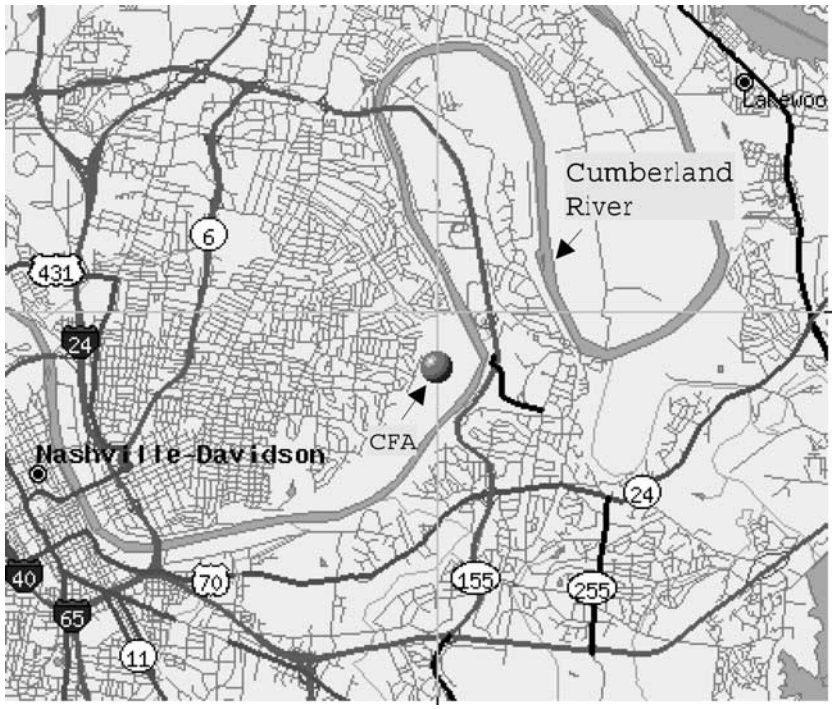

Figure 1. Map of region near the city of Nashville, Tennessee, showing the location of Cornelia Fort Airpark (CFA), indicated by the circle in the center of the map. The distance between downtown Nashville and CFA is ~10 km. The Cumberland River and major highways are shown.

local scales, was a key objective. Investigating PBL dynamics, including vertical transport and mixing of ozone and its precursors throughout the diurnal cycle, particularly during the morning and evening transition times, was another key objective. Since stable boundary layer meteorology and nighttime chemistry have received far less attention in previous studies than daytime processes, the SOS 1999 field campaign was designed to include extensive nighttime measurements in order to increase our understanding of what happens to ozone and its precurors at night. The LLJ, an elevated layer of relatively stronger wind flow, is a nighttime phenomenon that plays a critical role in nighttime transport [*Banta et al.*, 1998] and was a major feature of interest to SOS 1999 investigators. Additional PBL dynamics issues included documenting the reservoir of ozone that may develop in the evening hours and determining how that reservoir of ozone may affect pollution levels the next day. The Cornelia Fort Airpark (CFA), a heavily instrumented ground site for the campaign 10-km east-northeast of downtown Nashville, served as a focal point for much of the PBL research. In this paper, analysis of measurements from key instruments deployed at CFA will document two sudden increases in surface ozone detected on 22 June 1999. The first event, the major focus of this study, occurred in early evening. The second, less dramatic and not as well represented in the measurements, occurred after sunset.

[4] During the SOS 1999 field campaign, ozone measurements above the surface at CFA were available from a ground-based ozone profiling lidar, the Ozone Profiling Atmospheric Lidar (OPAL). Nearly continuous vertical profiles of ozone, measured by OPAL, combined with in situ measurements of ozone 10 m above ground level (AGL), showed the changes in the vertical gradient of ozone that occurred throughout the afternoon and early evening of 22 June 1999.

[5] In the afternoon, a residual layer (RL) of ozone formed as surface ozone concentrations declined to ~60 ppbv, but ozone concentrations above 400 m AGL remained relatively constant, with values near 90 ppbv. (Detailed measurements of these events are presented in section 4.) Later that evening a gust front (thunderstorm outflow) passed over CFA. After the gust front passage, ozone profiles showed a significant reduction in the vertical gradient of ozone. Ozone concentrations at 10, 405, and 1035 m AGL became within a few ppbv of each other. A rapid rise in ozone concentration of 20 ppbv, too rapid to be caused by chemical processes, occurred at 10 m AGL, whereas ozone concentrations at 405 and 1035 m dropped ~15 ppbv, indicating downward mixing of ozone. The higher surface ozone concentrations were maintained for about an hour after the gust front passage.

[6] Measurements of the horizontal and vertical structure of the gust front winds and subsequent formation of a LLJ were obtained from a high-resolution Doppler lidar collocated with OPAL, providing information about the mixing and transport that occurred during and after the gust front passage. Analysis of measurements from the Doppler and ozone profiling lidars, combined with measurements from a collocated sonic anemometer, radar wind profiler, and a meteorological surface station, explain mechanisms responsible for the vertical variations in ozone before and after the gust front, and a second rise in surface ozone occurring ~2 hours after the gust front passage.

[7] In section 2, the instrumentation and experiment site are briefly described. In section 3, Doppler lidar measurements documenting various stages of the gust front are

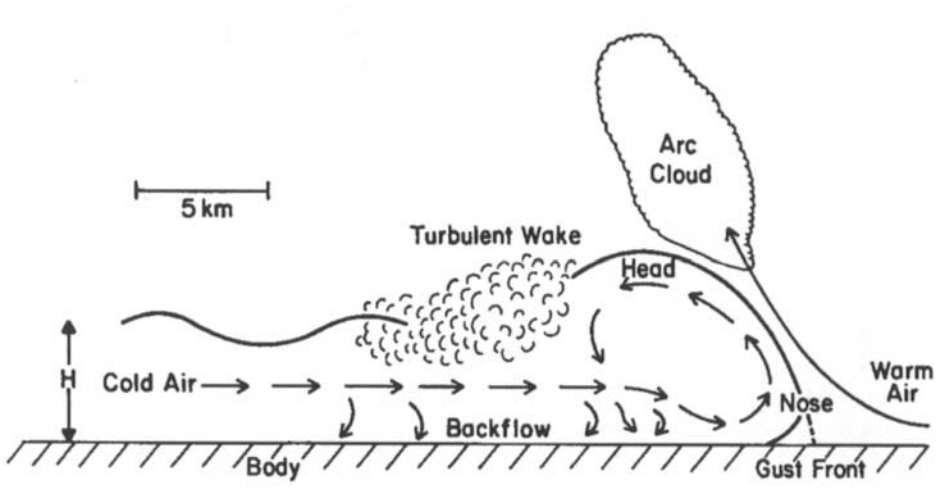

Figure 2. Conceptual model of a thunderstorm outflow, from *Droegemeier and Wilhelmson* [1987].

presented. Section 4 includes time series of measurements covering a 6-hour time span centered upon the gust front passage. In section 5 the key results are summarized.

2. Instrumentation and Site

[8] CFA lies in the Cumberland River valley (Figure 1). Major highways lie within 10 km of CFA in all directions, but the closest highway is ~2 km east of CFA. The Cumberland River flows between CFA and the highways to the south and east. All measurements presented in this study were from instruments placed within ~200 m of the lidars at CFA. The 10-m ozone sensor and the radar wind profiler were deployed by the National Oceanic and Atmospheric Administration/Aeronomy Laboratory (NOAA/AL). The remaining instruments, as discussed below, were deployed by the NOAA/Environmental Technology Laboratory (NOAA/ETL). The ozone profiling lidar, OPAL [*Zhao et al.*, 1993], and the minimaster-oscillator, power amplifier (mini-MOPA) Doppler lidar [*Brewer et al.*, 1998] were placed only 10 m apart. For the duration of the time period presented here, OPAL was pointing vertically, measuring ozone from 405 to 1400 m AGL, with a range resolution of 90 m. The Doppler lidar measured the radial winds with a variety of constant-elevation-angle and constant-azimuth-angle scans, which were either standard routine survey scans or scans implemented in real time according to the wind flows detected. The along-beam

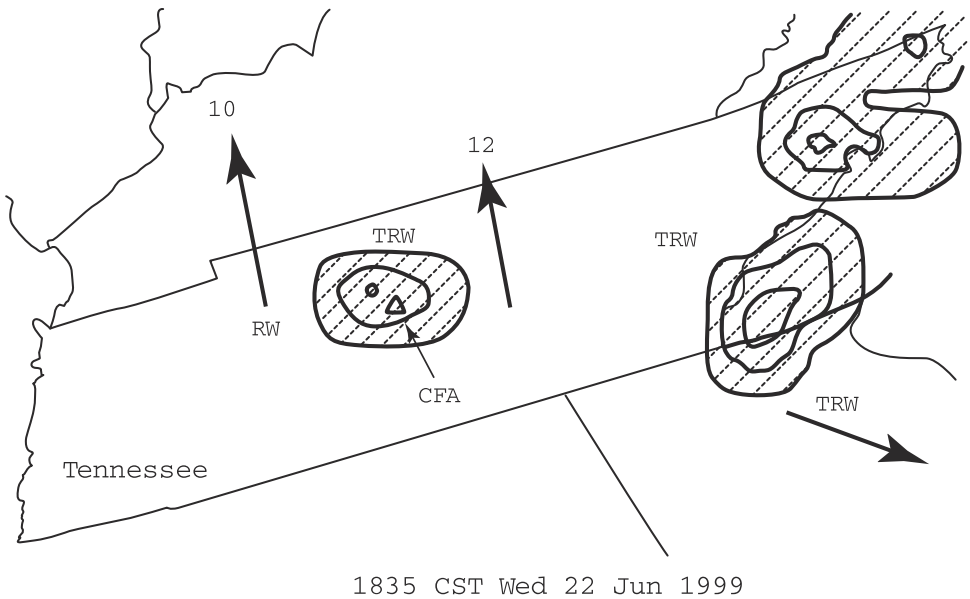

Figure 3. Radar map at 1835 CST, 22 June 1999 (0035 UTC, 23 June 1999) provided by the National Climatic Data Center. Location of CFA is marked with a triangle. The map indicated a thunderstorm was moving to the north from the Nashville area at 1835 CST, 22 June 1999. The contours indicate three levels of rainfall rates: weak to moderate; strong to very strong; and intense to extreme. Arrows and numbers indicate storm motion in knots. TRW indicates thunderstorm, and RW indicates rain shower.

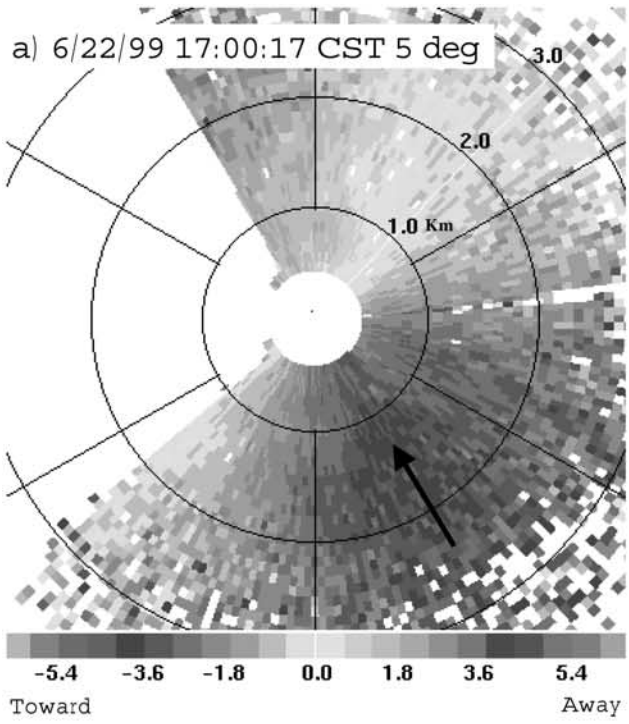

Pre-frontal southeasterly flow

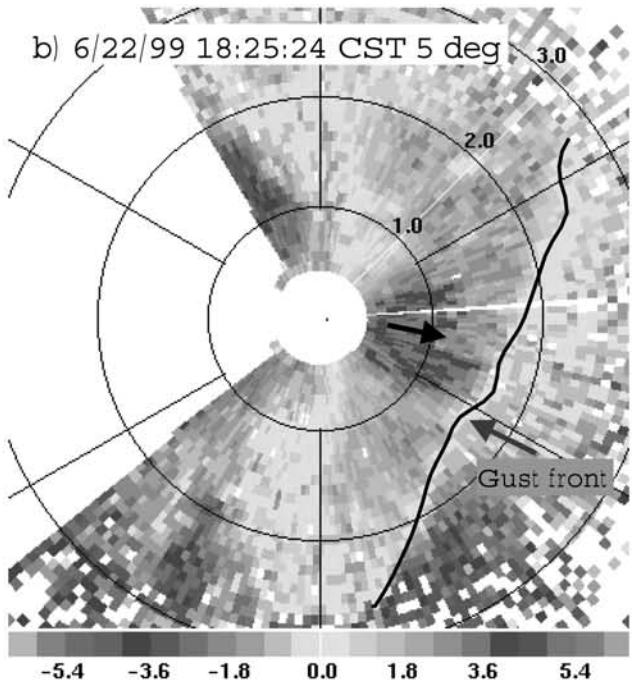

~10 min after gust front passage

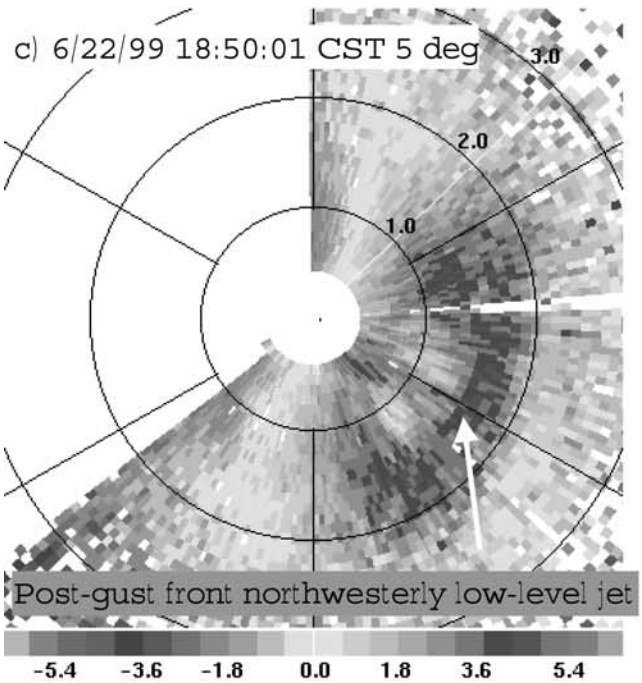

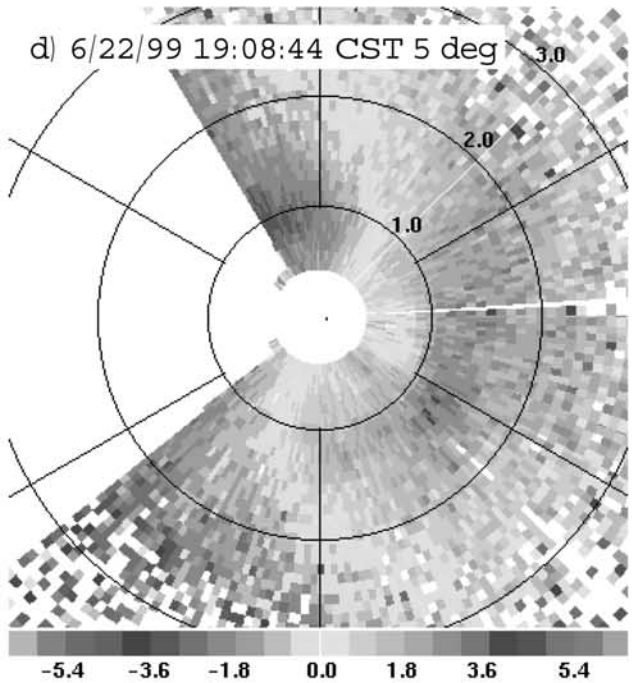

Low-level jet has dissipated

resolution of the Doppler measurements was 90 m. The sonic anemometer and the prop-vane anemometer were mounted on a 10-m tower ~50 m north of the lidars. The prop-vane anemometer winds were measured at 10 m AGL and were recorded the last second of every minute. Data from the sonic anemometer, mounted at 8 m AGL, are 1-s averages of 20-Hz data. The 10-m ozone measurements using the NO/O_3 chemiluminescence method were taken ~25 m north of the tower. The 915-MHz radar wind profiler was farthest away from the lidars, ~200 m to the south.

3. Lidar Measurements of the Gust Front and Low-Level Jet

[9] When a thunderstorm downdraft reaches the ground, it spreads out radially [*Mueller and Carbone*, 1987]. Since the sinking air is cooled evaporatively, becoming cooler than the ambient air, the outflow behaves as a density current [*Charba*, 1974] and can propagate for tens of kilometers away from the thunderstorm [*Wakimoto*, 1982]. Figure 2 [from *Droegemeier and Wilhelmson*, 1987] shows a conceptual model of a gust front. Several features of the outflow seen in Figure 2 contribute to vertical mixing and horizontal transport. The vertical motion ahead of the front, the turbulent wake region, and the recirculation within the head of the front are all potential mechanisms for vertically redistributing pollutants.

[10] Measurements of outflows have traditionally been made by Doppler radars, meteorologically instrumented towers, radiosondes, and surface stations (see *Wakimoto* [1982], *Mueller and Carbone* [1987], *Klingle et al.* [1987], *Mahoney* [1988], and *Martner* [1997] for examples). Doppler lidar is well suited for measuring the horizontal winds associated with front passages, outflows, and density currents in great detail [*Intrieri et al.*, 1990; *Olivier et al.*, 1998; *Darby et al.*, 1999, 2000]. In this section, we present lidar scans revealing both the horizontal and vertical structure of the gust front that passed through CFA, propagating into opposing ambient flow, and revealing some of the features shown in Figure 2. Figure 3 is a radar reflectivity map from 1835 CST showing thunderstorm echoes in the state of Tennessee. The gust front propagated from the thunderstorm northwest of CFA. Even though the location of CFA was within the radar echo, no rain fell at CFA during the period presented in this paper.

[11] Figure 4 is a series of Doppler lidar radial-velocity conical scans taken at a constant elevation angle of 5° above the horizon. The 2-km range ring thus represents measurements at a height of ~170 m AGL. Green and blue (negative radial velocities) represent flow toward the lidar, whereas yellow and red (positive radial velocities) represent flow away from the lidar. Figure 4a shows prefrontal southeasterly flow, with a slight increase in wind speed with height. Figure 4b shows the winds ~10 min after the gust front passage. The boundary between the gust front and the ambient air mass (indicated by the solid black line) was quite well defined. By 1850 CST (Figure 4c) the gust front had nearly moved out of the lidar's maximum range, the northwesterly flow had become deeper, and the weak LLJ (elevated region of red radial velocities) was well established. With time, the LLJ weakened and the northwesterly winds became more uniform with height (Figure 4d).

[12] Range-height scans along a constant azimuth are shown in Figure 5. The top two scans were routine survey scans at 150° azimuth, during which time the gust front was detected. After switching to conical scans, we found that 100° was a more appropriate azimuth angle for scanning through the gust front (see Figure 4b), so the remaining four range-height scans shown were at that angle. The leading edge of the outflow (indicated by a red arrow) was very evident in Figures 5a and 5b. In Figures 5c and 5d the head and turbulent wake region were prominent. In Figures 5e and 5f the gust front was beyond the lidar's maximum range, but we see the LLJ at 1852 CST (Figure 5e). The flow with a westerly component became fairly uniform with height by 1921 CST (Figure 5f), consistent with the scans shown in Figure 4.

[13] Features of the gust front that most likely affected the distribution of pollutants at CFA included the introduction of a new air mass behind the gust front; upward vertical motion at the leading edge of the outflow; downward vertical motion behind the head; mixing between air masses in the turbulent wake; transport due to the LLJ; and more uniform winds with height after the dissipation of the LLJ. These features will be addressed in the remainder of this section and provide a context for the postgust front portion of the time series discussion in section 4.

3.1. Introduction of a New Air Mass

[14] The introduction of a new air mass behind the gust front may play a role in the increase of surface ozone associated with the gust front. Since the outflow originated from a thunderstorm, and it has been shown previously that thunderstorm outflows can contain higher ozone levels [*Winterrath et al.*, 1999], we cannot completely rule out horizontal transport as a factor. However, we do not have upstream ozone data to determine whether this was the case.

3.2. Vertical Velocities

[15] According to *Wakimoto* [1982], the vertical velocities w associated with a gust front can be calculated from Doppler radar data using the equation of continuity if the density variation with height can be ignored and if the flow is two dimensional. He shows that both assumptions are valid in the case of a gust front. He also points out that since the winds behind the gust front are generally perpendicular

Figure 4. (opposite) Doppler lidar radial velocity measurements from scans at a 5° elevation angle. Negative velocities indicate flow toward the lidar, and positive velocities indicate flow away from the lidar. The lidar is positioned in the center of each scan. Range rings are in 1 km increments. North is to the top of each plot. The data gap to the west was caused by beam blockage from buildings and terrain: (a) 1700:17 CST, prefrontal southeasterly flow, (b) 1825:24 CST, gust front (solid black line) propagating into opposing flow, (c) 1850:01 CST, postgust front low-level northwesterly jet (position of jet indicated by white arrow), and (d) 1908:44 CST, fairly uniform winds with height. See color version of this figure at back of this issue.

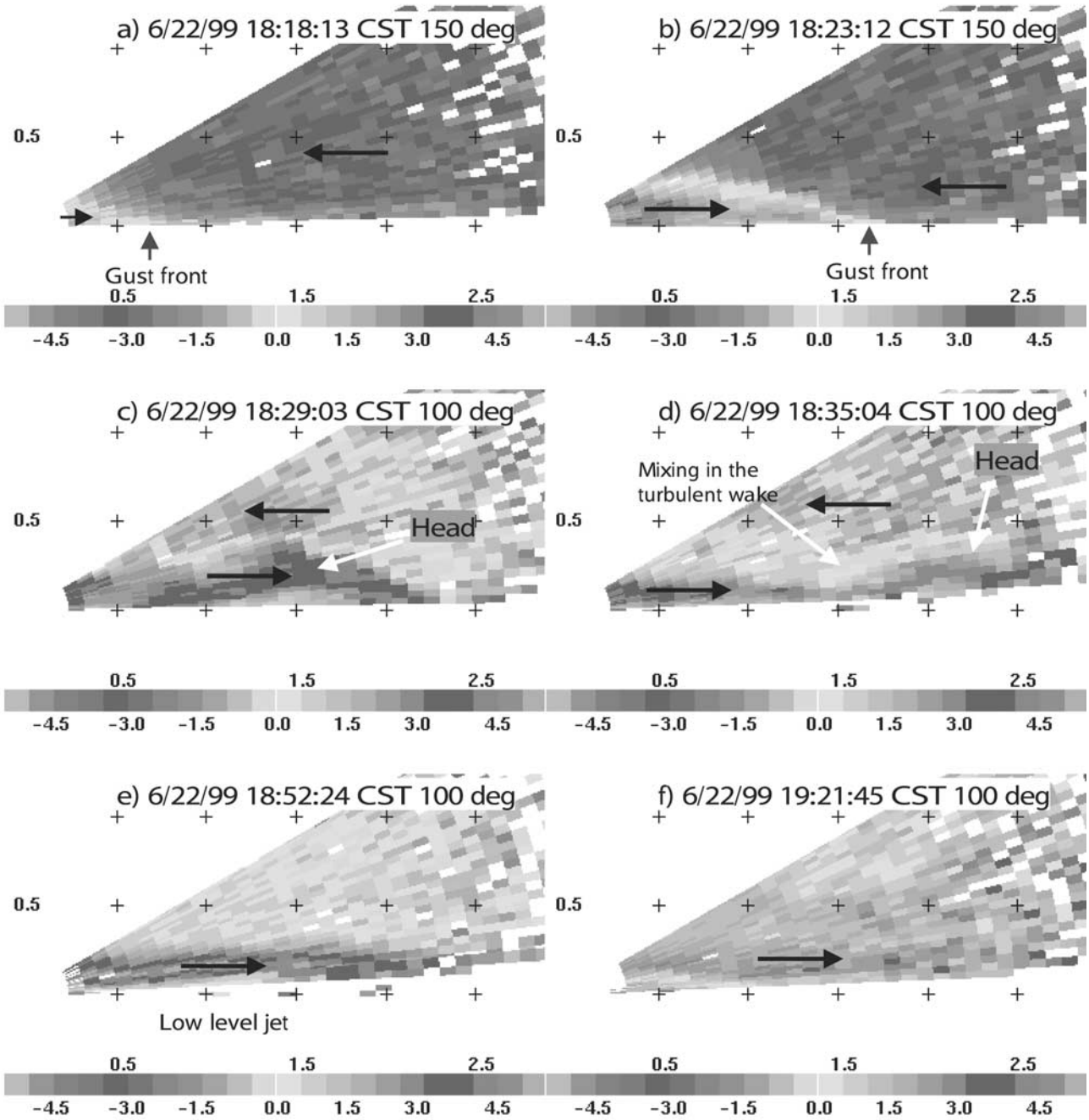

Figure 5. Vertical cross sections of Doppler lidar radial velocity measurements at constant azimuth angles. The lidar is positioned at $x = y = 0$ (lower left corner of each plot). Tick marks are in 0.5-km increments. Black arrows indicate the direction of the wind flow (negative velocities indicate flow toward the lidar, and positive velocities indicate flow away from the lidar): (a) 1818:13 CST, 150° azimuth. Leading edge of the gust front is marked with a red arrow; (b) 1823:12 CST, 150° azimuth. Leading edge of the gust front is marked with a red arrow; (c) 1829:03 CST, 100° azimuth. Head of the gust front is marked with a white arrow; (d) 1835:04 CST, 100° azimuth. Turbulent wake region behind the head is indicated with a white arrow; (e) 1852:24 CST, 100° azimuth. The low-level jet is indicated by the slightly elevated region of red and pink velocities; (f) 1921:45 CST, 100° azimuth, fairly uniform northwesterly flow. See color version of this figure at back of this issue.

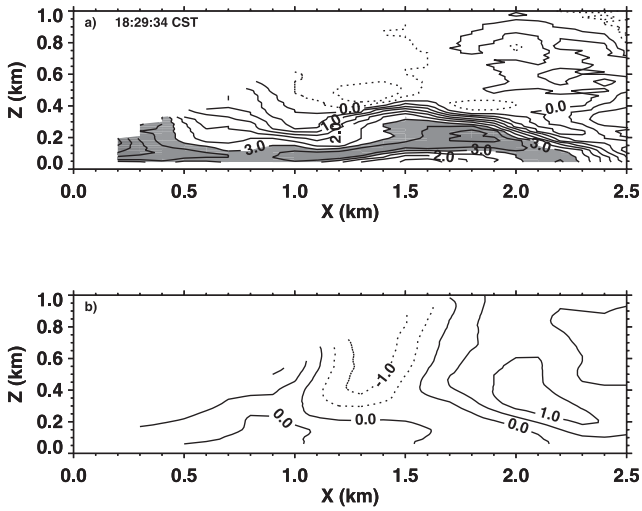

Figure 6. (a) Contours of the horizontal component of the wind parallel to the plane of a single vertical-slice scan, which was pointing along the 100° radial. Start time of the scan was 1829:34 CST. Solid contours indicate flow with a northwesterly component, and dashed contours indicate flow with a southeasterly component. Winds greater than 3 m s^{-1} are shaded. (b) Inferred vertical velocities calculated from the winds shown in Figure 6a. Solid contours represent upward vertical motion, and dashed contours indicate downward vertical motion. In both plots the contour increments are 0.5 m s^{-1} and the zero contour is bold. The *x* and *z* distances are relative to the lidar.

to the front, scanning normal to the front at low angles is an adequate measure of the horizontal gust front winds. More recently *Banta et al.* [1992] and *Intrieri et al.* [1990] used the same technique with Doppler lidar data.

[16] Mini-MOPA Doppler lidar scans at 100° azimuth comply with Wakimoto's criteria, and lidar data can be processed in the same manner as radar data. Figure 6a is a plot of the horizontal component of the wind parallel to the plane of a single range-height scan at 100° azimuth (similar to the scan shown in Figure 5c). The data were converted from polar to Cartesian coordinates, and to obtain the horizontal component of the wind, the radial velocity was divided by the cosine of the elevation angle of the beam. Winds >3 m s^{-1} have been shaded to highlight the vertical structure of the gust front flow and the elevated stronger winds. Note that the outflow was close to 400 m deep.

[17] Figure 6b shows the inferred *w* values calculated via the mass continuity equation using the horizontal winds shown in Figure 6a. The inferred *w* values showed upward vertical velocities ahead of the gust front and downward vertical velocities behind the head, with values >1 m s^{-1}. The negative *w* values extended down to the surface, but the strongest values were at and above 400 m. These results showing an elevated downward maximum behind the head of the gust front agree with *Ralph et al.* [1993], who found maximum *w* values near 3 m s^{-1} above 1 km AGL with sodar and radar wind profiler measurements, and with *Martner*'s [1997] direct measurements of gust front vertical velocities by radar. *Martner*'s [1997] results show an updraft maximum at 1.35 km AGL and a downdraft maximum of 9.9 m s^{-1} 1 min later at 1.46 km AGL. Our measurements do not extend as high above ground, so we do not know whether stronger *w* values occurred above the region we measured. It is enough to know, however, that strong downward motion occurred behind the gust front above 400 m near 1830 CST, and the downward motion extended down to the ground. Sonic anemometer data (shown in the next section) also indicated strong postgust front vertical velocities. These *w* values were strong enough to cause significant vertical mixing, resulting in the downward transport of ozone.

3.3. Mixing Between Air Masses

[18] Figure 5d shows an example of the winds that cause mixing in the turbulent wake region behind the head of a gust front. Note the ragged interface between the gust front and ambient air masses, as indicated by the frequent changes in sign of the radial velocities between 200 and 500 m AGL. This mixing between air masses most likely contributed to well-mixed ozone concentrations.

3.4. Transport Due to the LLJ

[19] A possible consequence of the presence of the LLJ is enhanced horizontal transport of pollutants into and out of CFA within the jet. Doppler lidar data (not shown) indicated that the LLJ was 100 to 300 m AGL, but since the lowest level of OPAL ozone measurements was 405 m AGL, we do not have a time series of ozone within the jet to assess the horizontal transport. The vertical mixing that occurred underneath the LLJ will be discussed in the next section.

3.5. Uniform Winds With Height

[20] As the LLJ dissipated, the northwesterly winds became more uniform with height and were fairly weak (mostly < 3 m s^{-1}, Figure 5d). As will be shown in the next section, as the horizontal and vertical variability in the winds diminished, the turbulent mixing became greatly reduced. Thus this change in the vertical structure of the winds may have aided in the re-formation of an RL, as ozone at 10 m began to decline and ozone concentrations aloft remained high.

4. Time Series Measurements

[21] Figure 7 shows time series of chemical and meteorological variables related to the behavior of the gust front. After a brief description of what each of the panels represent, we discuss each period in the time line at the top of Figure 7.

[22] The time series in Figure 7 include ozone concentrations at 10, 405, and 1035 m AGL (Figure 7a), standard deviation of the vertical wind speed σ_w at 8 m AGL (Figure 7b), vertical wind *w* 8 m AGL (Figure 7c), the variance of the horizontal wind derived from lidar radial velocity measurements (Figure 7d), temperature at 8 m AGL (Figure 7e), and surface wind direction at 10 m AGL (Figure 7f). The vertical wind component (Figure 7c) was measured by the sonic anemometer, and the σ_w time series (Figure 7b) was derived from the *w* time series. From lidar radial velocity range-height scans along a constant azimuth (as in Figure 5) the horizontal component of the wind parallel to the plane of each lidar scan was calculated as explained in the previous section. The vertical resolution of the Cartesian grid was 15 m. The winds from each scan

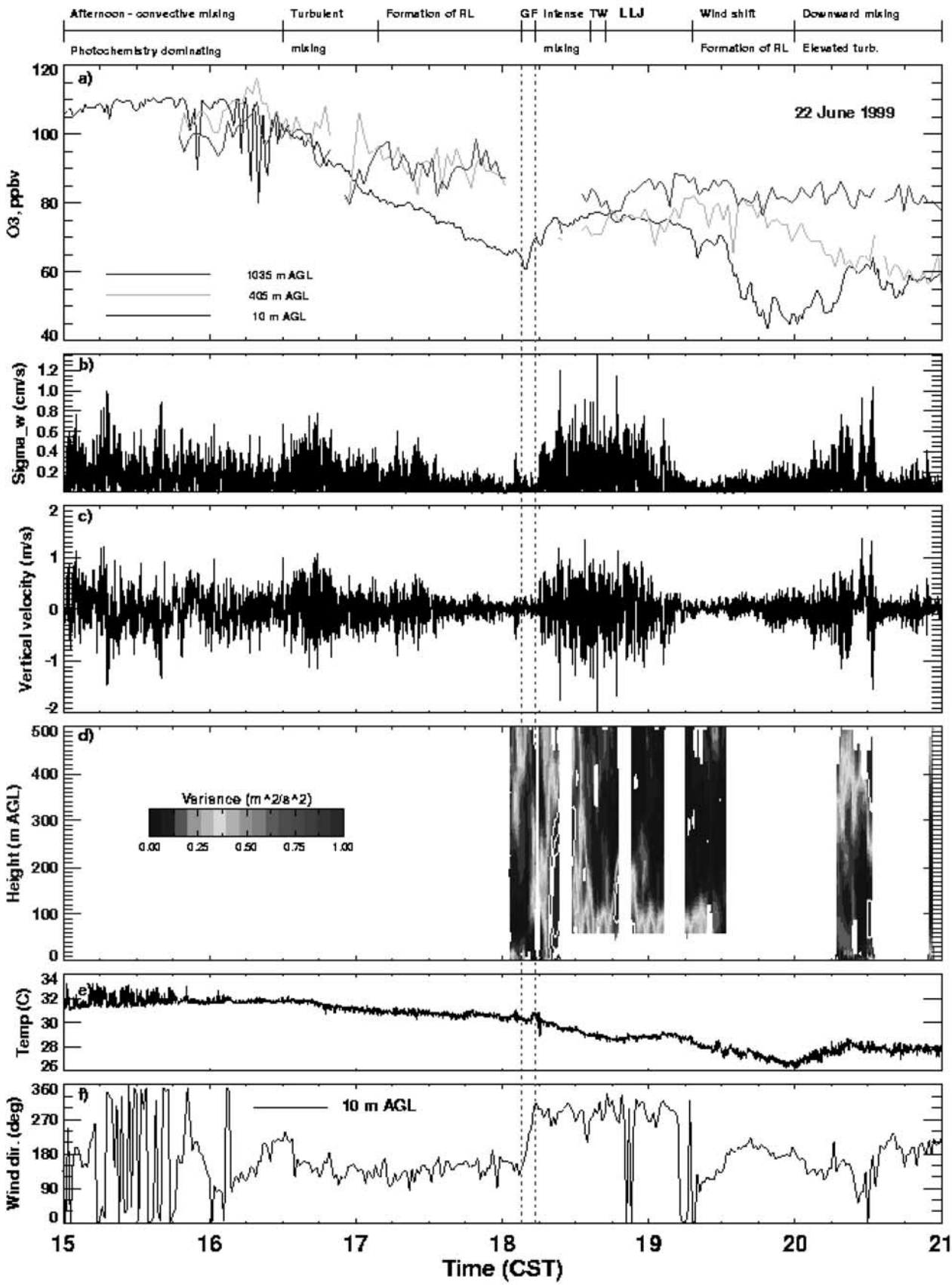
Afternoon - convective mixing
Turbulent
Formation of RL
GF
Intense TW
LLJ
Wind shift
Downward mixing
Photochemistry dominating
mixing
mixing
Formation of RL
Elevated turb.
a)
22 June 1999
O3, ppbv
1035 m AGL
405 m AGL
10 m AGL
b)
Sigma_w (cm/s)
c)
Vertical velocity (m/s)
d)
Height (m AGL)
Variance (m^2/s^2)
0.00
0.25
0.50
0.75
1.00
e)
Temp (C)
f)
Wind dir. (deg)
10 m AGL
15
16
17
18
19
20
21
Time (CST)

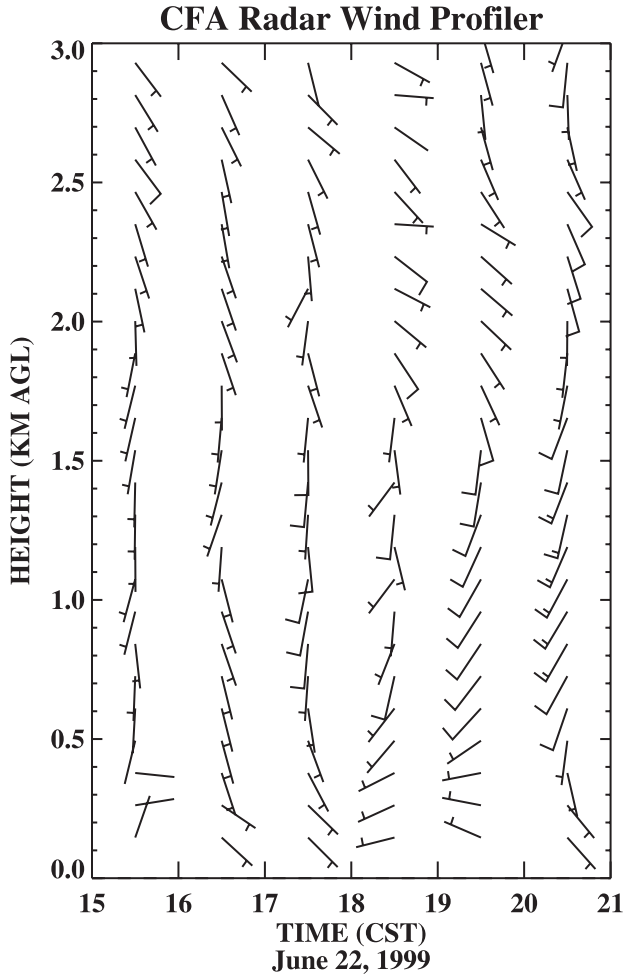

Figure 8. Hourly averaged winds from a 915-MHz radar wind profiler deployed at CFA. Half barbs are 2.5 m s^{-1}, and full barbs are 5 m s^{-1}. Profiles are plotted at the midpoint of the hour over which the winds were averaged.

were then horizontally averaged, creating a single vertical profile of the horizontal wind and its variance for each scan (technique further described by *Banta et al.* [2002]). All profiles were combined to create the time series in Figure 7d.

[23] The temperature time series (Figure 7e) was from the sonic anemometer. Over the entire period of interest, the surface prop-vane anemometer wind speed measurements were <3 m s^{-1}. These weak values did not show any trends that contributed to the analysis, so only the wind direction time series from this sensor will be shown. For additional wind information, hourly radar wind profiler data from CFA are shown in Figure 8.

4.1. Afternoon Convective Mixing

[24] High ozone concentrations during the late afternoon hours were accompanied by light and variable winds in the lowest 500 m, with light southerly winds above (1530 CST, Figure 8). The σ_w values indicated turbulent mixing near the surface, and the magnitude of w values occasionally exceeded 1 m s^{-1} both upward and downward. Photochemical production of ozone was a dominating mechanism at this time, and the afternoon convective mixing kept ozone levels high throughout a deep layer, as seen in the OPAL measurements (red and green traces). The sharp variations in the 10-m ozone trace between 1545 and 1630 CST were a result of NO_x emissions from rush-hour traffic being advected over CFA from nearby highways. Similar variations in the NO_x time series (not shown) were anticorrelated with the ozone measurements. By 1630 CST the winds shifted to southeasterly in a deep layer (Figure 8). Turbulent mixing continued to dominate, as ozone concentrations at all three levels became similar in value. The late afternoon decline in low-level ozone had begun.

4.2. Formation of Residual Layer

[25] Light southeasterly flow became established after 1700 CST. Turbulent mixing began to decrease, as evidenced by decreases in w and σ_w. Ozone values at 10 m continued to steadily decline, whereas ozone at 405 and 1035 m remained relatively constant, close to 90 ppbv. These trends resulted in a typical light-wind evening ozone profile, with lower concentrations near the surface and higher concentrations aloft (the RL).

4.3. Gust Front Passage With Intense Vertical Mixing

[26] The formation of the residual layer continued until just after 1800 CST, when the gust front approached CFA. The beginning and end of the surface wind shift from southeast to northwest caused by the gust front passage are marked by the vertical red dotted lines on Figure 7. OPAL was not recording data when the gust front passed over CFA, so there was a gap in the upper-level ozone measurements surrounding the passage. As the wind was shifting, surface ozone increased by ~10 ppbv.

[27] After the wind shift was complete, w and σ_w values increased, indicating low-level turbulent mixing. The surface ozone concentration again increased by ~10 ppbv as a result of the enhanced downward mixing. The lidar horizontal wind variance increased dramatically after the gust front passage, with high values extending from near the surface to 500 m AGL, indicating turbulent mixing through a layer at least 500 m deep. The deep vigorous mixing

Figure 7. (opposite) Time series of (a) ozone concentrations (ppbv) at 10, 405, and 1035 m AGL; (b) standard deviation of the vertical wind speed, σ_w at 8 m AGL (cm s^{-1}); (c) vertical wind speed, w at 8 m AGL (m s^{-1}); (d) variance of the lidar-measured horizontal wind (m^2 s^{-2}); (e) temperature at 8 m AGL (°C); and (f) wind direction at 10 m AGL (degrees true north). Measurements are described in the text. For Figure 7d the color scale stops at 1 m^2 s^{-2} in order to maximize use of the scale to reveal the structure of the lower variance values. Values between 1 and 3 m^2 s^{-2} are contoured in white in increments of 1 m^2 s^{-2} to delineate the structure of the higher variance values. Abbreviations used in the time line: residual layer (RL), gust front (GF), turbulent wake region (TW), and low-level jet (LLJ). See color version of this figure at back of this issue.

lasted for ~15 min before decreasing in-depth and intensity (Figure 7d). The reduction in ozone concentrations at 1035 m, however, indicated that strong mixing occurred throughout at least the lowest 1 km AGL. The Doppler-lidar- inferred *w* values seen in Figure 6b (showing the maximum downward vertical velocities above 400 m AGL), indicated downward motion strong enough to keep the PBL well mixed at this time (1830 CST).

4.4. Turbulent Wake Region

[28] Figures 2 and 5d show a turbulent wake region behind the gust front head. This structure of the winds has been attributed to Kelvin-Helmholtz instability [*Mueller and Carbone*, 1987; *Droegemeier and Wilhelmson*, 1987]. Although the turbulent wake region portion of the time line was quite short, it was a significant period of vertical mixing. Both the maximum downward *w* and maximum σ_w values occurred during this time (Figures 7b and 7c). The elevated nature of the turbulent wake region may have enhanced the depth of the mixing.

4.5. Low-Level Jet

[29] Behind the gust front a LLJ formed (the elevated layer of relatively stronger winds in Figure 5e). During this LLJ period the ozone concentrations at 10 and 405 m remained nearly equal in value (1845 to 1900 CST), with a very gradual decline at 10 m. This decline coincided with a second period of strong mixing during the first half of the LLJ phase of events, as indicated by a period of high lidar variances up to 200 m AGL between ~1845 and 1900 CST. This observation is consistent with *Reitebuch et al.* [2000], who show increased σ_w between the surface and the core of a LLJ, causing a jump in surface ozone concentration as a result of downward mixing. Thus, after the initial deep mixing by mechanically driven turbulence caused by the gust front passage and the turbulent wake region, the turbulent mixing below the jet served to keep the lowest 200 m well mixed (as indicated by lidar variances, Figure 7d). Ozone concentrations were similar at 10 and 405 m, however, indicating either that the mixing was deeper than indicated by the lidar variances, or that horizontal transport was a factor.

4.6. Wind Shift and Formation of Residual Layer

[30] With the dissipation of the LLJ the lower-level winds returned to the pregust-front southeasterly flow, as indicated by the surface data (Figure 7f) and the radar wind profiler data (1930 CST, Figure 8). With the more uniform winds, i.e., less horizontal and vertical shear, both *w* and σ_w decreased with time as the LLJ dissipated. Surface ozone values had a sharp decline between 1930 and 2000 CST, following the wind shift. NO_x time series (not shown) showed a rise in NO_x coincident with the wind shift, indicating that NO_x was advected into CFA, and therefore the titration of ozone was the dominating mechanism in the steep decline in surface ozone concentrations. Deposition probably also played a role in the decline. Toward the end of this period, the ozone at 405 m began decreasing slightly. Evening declines of ozone in the residual layer such as this are most likely caused by downward mixing of ozone [*Neu*, 1995].

4.7. Elevated Turbulence and Downward Mixing

[31] A second jump in surface ozone concentration occurred at ~2015 CST followed by a wind direction shift at the surface (Figure 7f), enhanced mixing as seen in σ_w (Figure 7b), and a postsunset increase in temperature (Figure 7e). Mini-MOPA lidar data (not shown) indicated an intruding layer of flow ~500 m AGL in opposition to the ambient winds. These opposing winds descended toward the surface with time. While the meteorology behind this feature cannot be determined from the data we have, the resultant turbulence is evident in the measurements. *Reitebuch et al.* [2000] and *Nappo* [1991] also saw a nocturnal temperature rise coincident with a surface ozone concentration jump and attribute the temperature increase to downward turbulent mixing. Wind profiler data (Figure 8) showed a directional shear layer between 300 and 500 m AGL at this time. Lidar variances showed that the greatest turbulent mixing occurred above 300 m. The consistency between the 405- and 10-m ozone measurements indicated that although the mixing mechanism was elevated, the effect of the mixing reached the surface. Additionally, ozone measurements at 1035 m remained unchanged during this sequence of events, suggesting that the mixing was confined to a layer less than 1000 m deep.

5. Summary

[32] The unique set of instruments deployed at CFA provided an unprecedented combination of measurements to analyze the variations in ozone that occurred before and after a gust front passage on 22 June 1999. Nearly continuous time series of ozone at three heights, obtained from surface chemistry and OPAL measurements, showed many changes in ozone concentrations with both time and height. Ozone measurements above the surface confirmed the existence of a residual layer of ozone-rich air from which ozone could be mixed downward, raising ozone concentrations at the surface. The measurements extended through the evening transition (i.e., sunset occurred during the time period analyzed), one of the times of particular interest to SOS investigators.

[33] The scanning mini-MOPA Doppler lidar detected a gust front in real time, and scans were quickly implemented to measure the gust front's horizontal and vertical structure. Information from these scans contributed to the detailed analysis of the changes in ozone that occurred before and after the gust front passage. Doppler lidar measurements of the gust front revealed information such as the depth of the outflow, the structure of the head, the wake region behind the head, inferred vertical velocities, and a LLJ. The outflow depth was close to 400 m, which, if horizontal advection of higher-ozone air occurred, may explain in part why ozone values at 10 and 405 m were so similar after the gust front passage. The inferred lidar vertical velocities, however, combined with sonic anemometer measurements of *w*, and the reduction of ozone at 405 and 1035 m immediately following the gust front passage, indicated that the downward mixing of ozone-rich air was the dominant mechanism causing the changes in ozone that occurred after the gust front passage.

[34] We have shown that fluctuations in the vertical ozone profile resulted from shifts in the horizontal wind direction and the subsequent changes in the vertical wind component. These produced turbulent mixing and increases in surface ozone concentrations in two separate events.

Additionally, horizontal advection of NO_x-rich air contributed to a decrease in ozone concentrations at 10 m. By comparing the σ_w values from the sonic anemometer with the lidar variances of the horizontal wind, and assessing the accompanying changes in the vertical distribution of ozone, it has been shown here that changes in σ_w at 8 m can sometimes indicate mixing through a layer several hundred meters deep. The lidar variances indicated the depth and duration of strong turbulent mixing following the gust front and the low-level mixing associated with the LLJ.

[35] Gust fronts occur frequently during both day and night in the thunderstorm season, and are very likely to affect pollutants in a manner comparable to that presented in this paper. Similarly, large-scale and small-scale meteorological events that cause wind direction shifts and increased vertical velocities, and consequently vertical mixing, may also cause similar changes in the vertical gradient of ozone. However, it is also possible that the temperature difference between two air masses could be large enough that colder air flowing into a warm and unstable air mass will actually suppress turbulent mixing behind the front [*Bowen*, 1996]. Other meteorological events potentially affecting vertical transport include synoptic-scale front passages and LLJs, and density currents generated by sources other than thunderstorms. Vertical transport on a much larger scale, such as the downward transport of ozone from the stratosphere, is also associated with cold front passages [*Cooper et al.*, 1998]. In contrast to the downward transport of ozone associated with meteorological events the upward transport of ozone from the boundary layer to the free troposphere was documented by *Bethan et al.* [1998], who obtained aircraft ozone measurements in a developing baroclinic wave, and found higher ozone concentrations associated with the upward motion portion of the warm conveyor belt section of the wave. Thus a variety of meteorological processes can act to enhance vertical mixing between the earth's surface and the atmosphere in the manner described for the gust front in this study.

[36] **Acknowledgments.** The field deployment and research for the SOS 1999 study was funded by NOAA's Health of the Atmosphere program. The authors wish to thank Yanzeng Zhao for her contribution to the OPAL data collection.

References

Banta, R. M., L. D. Olivier, E. T. Holloway, R. A. Kropfli, B. W. Bartram, R. E. Cupp, and M. J. Post, Smoke column observations from two forest fires using Doppler lidar and Doppler radar, *J. Appl. Meteorol.*, *31*, 1328–1349, 1992.

Banta, R. M., et al., Daytime buildup and nighttime transport of urban ozone in the boundary layer during a stagnation episode, *J. Geophys. Res.*, *103*, 22,519–22,544, 1998.

Banta, R. M., R. K. Newsom, J. K. Lundquist, Y. L. Pichugina, R. L. Coulter, and L. J. Mahrt, Nocturnal low-level jet characteristics observed during CASES-99, *Boundary Layer Meteorol.*, in press, 2002.

Bethan, S., G. Vaughan, C. Gerbig, A. Volz-Thomas, H. Richer, and D. A. Tiddeman, Chemical air mass differences near fronts, *J. Geophys. Res.*, *103*, 13,413–13,434, 1998.

Bowen, B. M., Example of reduced turbulence during thunderstorm outflow, *J. Appl. Meteorol.*, *35*, 1028–1032, 1996.

Brewer, W. A., R. M. Hardesty, W. L. Eberhard, and B. J. Rye, Combined wind and water-vapor measurements using the NOAA mini-MOPA Doppler lidar, in *Proceedings of the 19th International Laser Radar Conference*, pp. 565–568, NASA Langley Research Cent., Hampton, Va., 1998.

Charba, J., Application of gravity current model to analysis of squall-line gust front, *Mon. Weather Rev.*, *102*, 140–156, 1974.

Cooper, O. R., J. L. Moody, J. C. Davenport, S. J. Oltmans, B. J. Johnson, X. Chen, P. B. Shepson, and J. T. Merrill, Influence of springtime weather systems on vertical ozone distributions over three North American sites, *J. Geophys. Res.*, *103*, 22,001–22,013, 1998.

Corsmeier, U., N. Kalthoff, O. Kolle, M. Kotzian, and F. Fiedler, Ozone concentration jump in the stable nocturnal boundary layer during a LLJ-event, *Atmos. Environ.*, *31*, 1977–1989, 1997.

Darby, L. S., W. D. Neff, and R. M. Banta, Multiscale analysis of a Meso-β frontal passage in the complex terrain of the Colorado Front Range, *Mon. Weather Rev.*, *127*, 2062–2081, 1999.

Darby, L. S., A. Gohm, L. B. Nance, S. Gabersek, R. M. Banta, and S. Sandberg, Foehn flow in the Austrian Alps interrupted by a cold front passage, Part I, in *Ninth Conference on Mountain Meteorology*, pp. 79–82, Am. Meteorol. Soc., Boston, Mass., 2000.

Droegemeier, K. K., and R. B. Wilhelmson, Numerical simulation of thunderstorm outflow dynamics, Part I, Outflow sensitivity experiments and turbulence dynamics, *J. Atmos. Sci.*, *44*, 1180–1210, 1987.

Intrieri, J. M., A. J. Bedard Jr., and R. M. Hardesty, Details of colliding thunderstorm outflows as observed by Doppler lidar, *J. Atmos. Sci.*, *47*, 1081–1098, 1990.

Klingle, D. L., D. R. Smith, and M. M. Wolfson, Gust front characteristics as detected by Doppler radar, *Mon. Weather Rev.*, *115*, 905–918, 1987.

Mahoney, W. P., Gust front characteristics and the kinematics associated with interacting thunderstorm ouflows, *Mon. Weather Rev.*, *116*, 1474–1491, 1988.

Martner, B. E., Vertical velocities in a thunderstorm gust front and outflow, *J. Appl. Meteorol.*, *36*, 615–622, 1997.

Mueller, C. K., and R. E. Carbone, Dynamics of a thunderstorm outflow, *J. Atmos. Sci.*, *44*, 1879–1898, 1987.

Nappo, C. J., Sporadic breakdowns of stability in the PBL over simple and complex terrain, *Boundary Layer Meteorol.*, *54*, 69–87, 1991.

Neu, U., A parameterization of the nocturnal ozone reduction in the vertical layer by vertical downward mixing during summer smog situations using SODAR data, *Boundary Layer Meteorol.*, *73*, 189–193, 1995.

Olivier, L. D., and G. S. Poulos, Frontal passage, mountain waves and flow reversals in the vicinity of the Colorado Springs, CO Airport, in *Preprints, 8th Conference on Mountain Meteorology, August 2–7, 1998, Flagstaff, AZ*, pp. 176–181, Am. Meteorol. Soc., Boston Mass., 1998.

Ralph, F. M., C. Mazaudier, M. Crochet, and S. V. Venkateswaran, Doppler sodar and radar wind-profiler observations of gravity-wave activity associated with a gravity current, *Mon. Weather Rev.*, *121*, 444–463, 1993.

Reitebuch, O., A. Strassburger, S. Emeis, and W. Kuttler, Nocturnal secondary ozone concentration maxima analysed by sodar observations and surface measurements, *Atmos. Environ.*, *34*, 4315–4329, 2000.

Wakimoto, R. M., The life cycle of thunderstorm gust fronts as viewed with Doppler radar and rawinsonde data, *Mon. Weather Rev.*, *110*, 1060–1082, 1982.

Winterrath, T., T. P. Kurose, A. Richter, and J. P. Burrows, Enhanced O3 and NO2 in thunderstorm clouds: Convection or production?, *Geophys. Res. Lett.*, *26*, 1291–1294, 1999.

Zhao, Y., J. N. Howell, and R. M. Hardesty, Transportable lidar for the measurements of ozone concentration and aerosol profiles in the lower troposphere, in *A&WMA/SPIE International Symposium on Optical Sensing for Environmental Monitoring*, pp. 310–320, Int. Soc. for Opt. Eng., Bellingham, Washington, 1993.

Zurita, E., and M. Castro, A statistical analysis of mean hourly concentrations of surface ozone at Madrid (Spain), *Atmos. Environ.*, *17*, 2213–2220, 1983.

W. M. Angevine and E. J. Williams, National Oceanic and Atmospheric Administration/Aeronomy Laboratory, Boulder, CO 80303, USA.

R. M. Banta, W. A. Brewer, L. S. Darby, and W. D. Neff, National Oceanic and Atmospheric Administration/Environmental Technology Laboratory, Boulder, CO 80305, USA.

R. D. Marchbanks, B. J. McCarty, C. J. Senff, and A. B. White, Cooperative Institute for Research in the Environmental Sciences, University of Colorado, Boulder, CO 80309, USA.

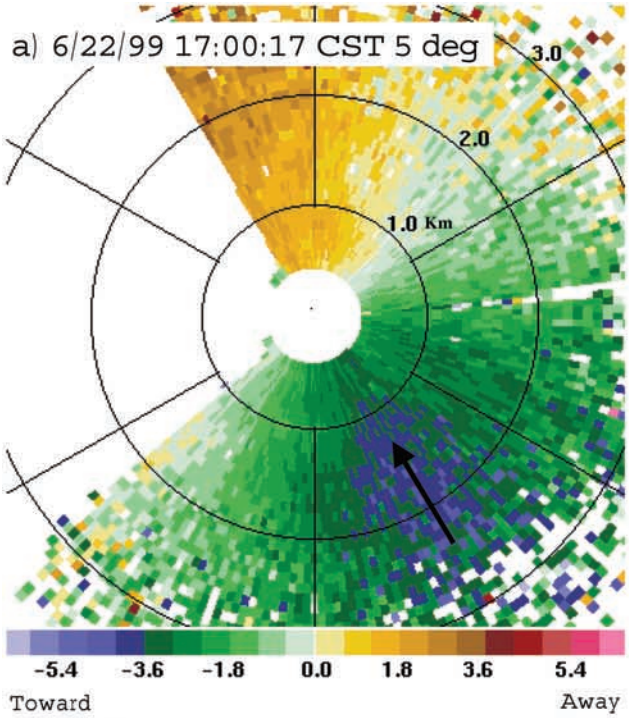

Pre-frontal southeasterly flow

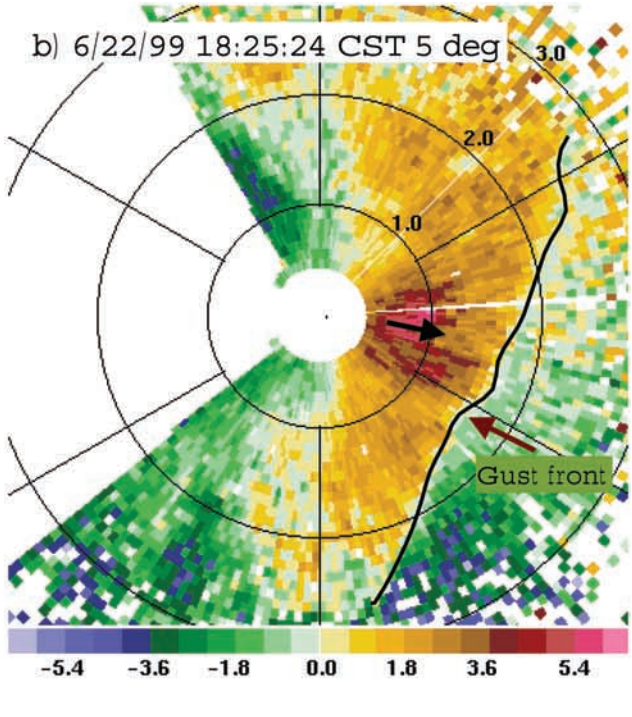

~10 min after gust front passage

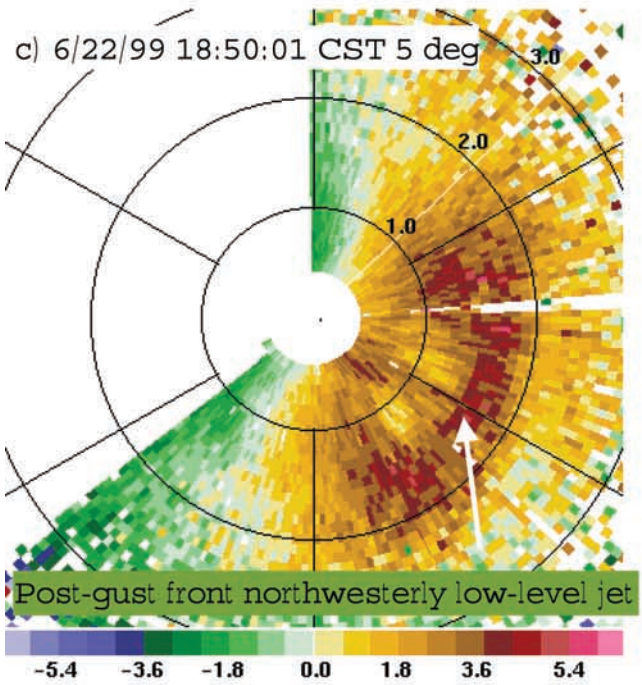

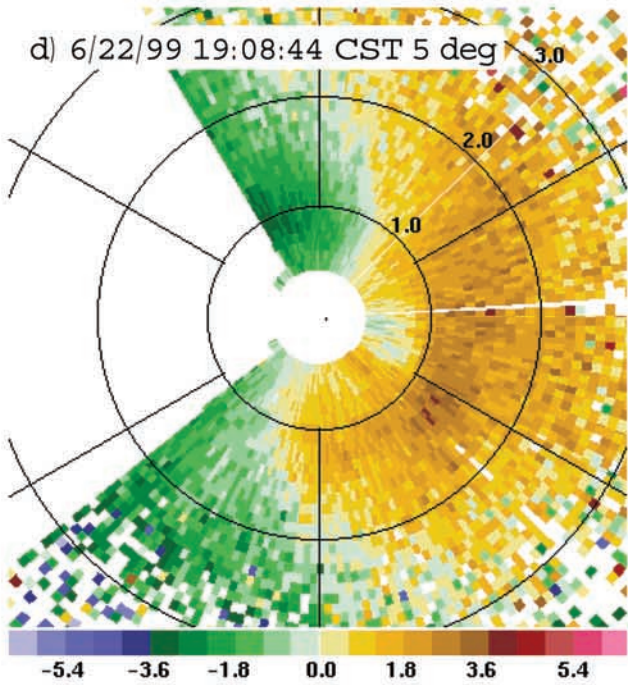

Low-level jet has dissipated

Figure 4. (opposite) Doppler lidar radial velocity measurements from scans at a 5° elevation angle. Negative velocities indicate flow toward the lidar, and positive velocities indicate flow away from the lidar. The lidar is positioned in the center of each scan. Range rings are in 1 km increments. North is to the top of each plot. The data gap to the west was caused by beam blockage from buildings and terrain: (a) 1700:17 CST, prefrontal southeasterly flow, (b) 1825:24 CST, gust front (solid black line) propagating into opposing flow, (c) 1850:01 CST, postgust front low-level northwesterly jet (position of jet indicated by white arrow), and (d) 1908:44 CST, fairly uniform winds with height.

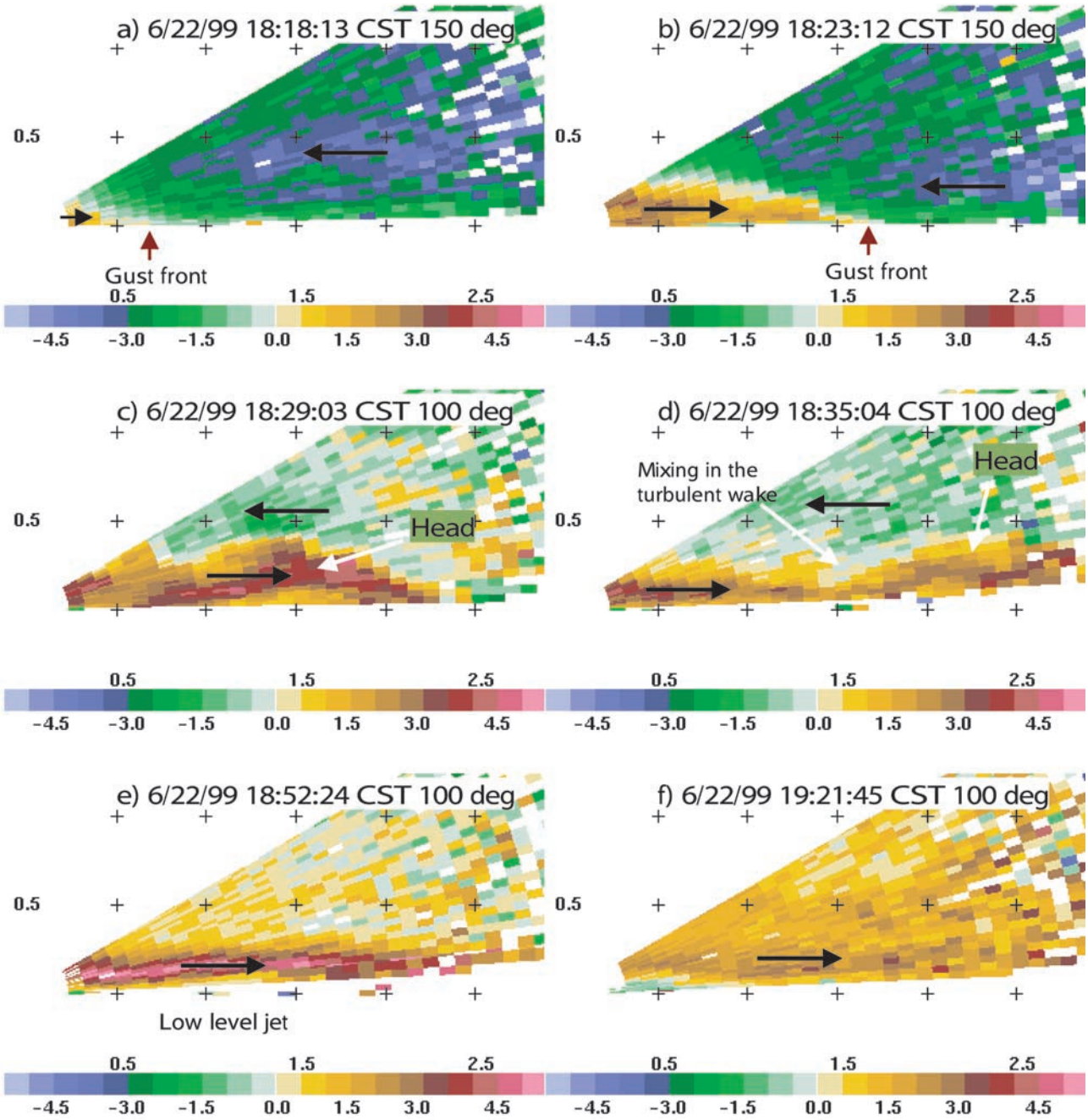

Figure 5. Vertical cross sections of Doppler lidar radial velocity measurements at constant azimuth angles. The lidar is positioned at $x = y = 0$ (lower left corner of each plot). Tick marks are in 0.5-km increments. Black arrows indicate the direction of the wind flow (negative velocities indicate flow toward the lidar, and positive velocities indicate flow away from the lidar): (a) 1818:13 CST, 150° azimuth. Leading edge of the gust front is marked with a red arrow; (b) 1823:12 CST, 150° azimuth. Leading edge of the gust front is marked with a red arrow; (c) 1829:03 CST, 100° azimuth. Head of the gust front is marked with a white arrow; (d) 1835:04 CST, 100° azimuth. Turbulent wake region behind the head is indicated with a white arrow; (e) 1852:24 CST, 100° azimuth. The low-level jet is indicated by the slightly elevated region of red and pink velocities; (f) 1921:45 CST, 100° azimuth, fairly uniform northwesterly flow.

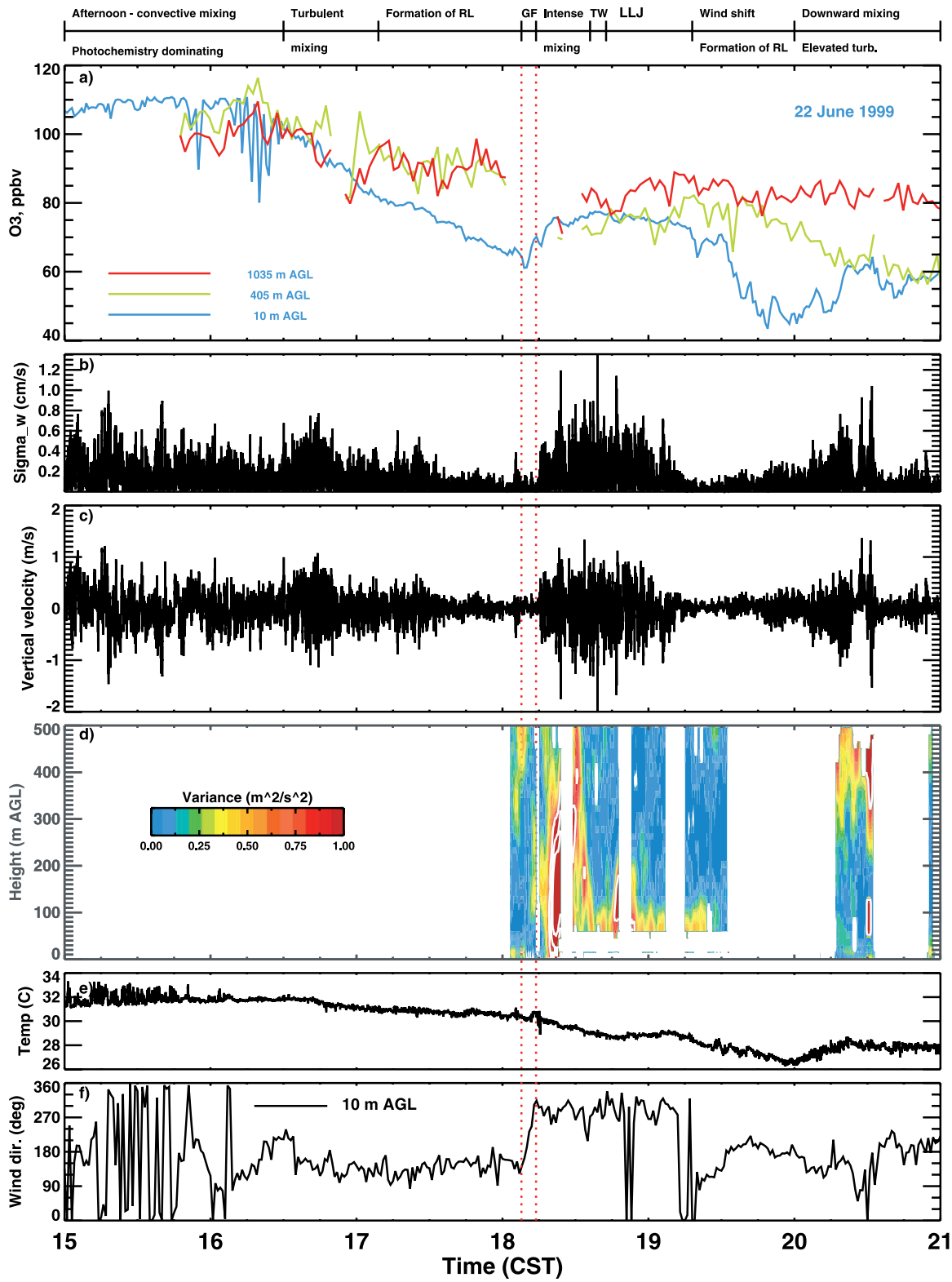
Afternoon - convective mixing
Turbulent mixing
Formation of RL
GF
Intense mixing
TW
LLJ
Wind shift
Formation of RL
Downward mixing
Elevated turb.
Photochemistry dominating
a)
22 June 1999
O3, ppbv
1035 m AGL
405 m AGL
10 m AGL
b)
Sigma_w (cm/s)
c)
Vertical velocity (m/s)
d)
Variance (m^2/s^2)
0.00
0.25
0.50
0.75
1.00
Height (m AGL)
e)
Temp (C)
f)
10 m AGL
Wind dir. (deg)
Time (CST)

Figure 7. (opposite) Time series of (a) ozone concentrations (ppbv) at 10, 405, and 1035 m AGL; (b) standard deviation of the vertical wind speed, σ_w at 8 m AGL (cm s^{-1}); (c) vertical wind speed, w at 8 m AGL (m s^{-1}); (d) variance of the lidar-measured horizontal wind (m^2 s^{-2}); (e) temperature at 8 m AGL (°C); and (f) wind direction at 10 m AGL (degrees true north). Measurements are described in the text. For Figure 7d the color scale stops at 1 m^2 s^{-2} in order to maximize use of the scale to reveal the structure of the lower variance values. Values between 1 and 3 m^2 s^{-2} are contoured in white in increments of 1 m^2 s^{-2} to delineate the structure of the higher variance values. Abbreviations used in the time line: residual layer (RL), gust front (GF), turbulent wake region (TW), and low-level jet (LLJ).